Ligand-directed Photocatalysts and Far-red Light Enable Catalytic Bioorthogonal Uncaging inside Live Cells

Julia Rosenberger,[1] Yixin Xie,[1] Yinzhi Fang,[1] Xinyi Lyu,[1] William S. Trout,[1] Olga Dmitrenko,[1] Joseph M. Fox *,[1]
[1] Department of Chemistry and Biochemistry, University of Delaware, Newark, Delaware 19716, USA

ABSTRACT: Described are ligand-directed catalysts for live-cell, photocatalytic activation of bioorthogonal chemistry. Catalytic groups are localized via a tethered ligand either to DNA or to tubulin, and red-light (660 nm) photocatalysis is used to initiate a cascade of DHTz-oxidation, intramolecular Diels-Alder reaction, and elimination to release phenolic compounds. Silarhodamine (**SiR**) dyes, more conventionally used as biological fluorophores, serve as photocatalysts that have high cytocompatibility and produce minimal singlet oxygen. Commercially-available conjugates of Hoechst dye (**SiR-H**) and Taxol (**SiR-T**) are used to localize **SiR** to the nucleus and tubulin, respectively. Computation was used to assist the design of a new class of redox-activated photocage to release either phenol or n-CA4, a microtubule-destabilizing agent. In model studies, uncaging is complete within 5 min using only 2 μM of **SiR** and 40 μM of the photocage. *In situ* spectroscopic studies support a mechanism involving rapid intramolecular Diels-Alder reaction and a rate determining elimination step. In cellular studies, this uncaging process is successful at low concentration of both the photocage (25 nM) and the **SiR-H** dye (500 nM). Uncaging n-CA4 causes microtubule depolymerization and an accompanying reduction in cell area. Control studies demonstrate that **SiR-H** catalyzes uncaging inside the cell, and not in the extracellular environment. With **SiR-T**, the same dye serves as photocatalyst and the fluorescent reporter for tubulin depolymerization, and with confocal microscopy it was possible to visualize tubulin depolymerization in real time as the result of photocatalytic uncaging in live cells.

Introduction

The localization and regulation of enzymes at the subcellular-level provides the foundation for the activity and behavior of cells. Mimicking nature's ability to control subcellular catalytic behavior represents an important challenge to the field of chemical biology.[1] Antibody-enzyme conjugates have been explored as a method for catalytically uncaging small molecules at the surface of tumor cells.[2] Related strategies based on catalytic antibodies,[3] gene therapy,[4] and CAR-T directed enzyme delivery[5] have also been described. Transition metal catalysis has also been developed as a way to uncage small molecules in cellular and in vivo systems.[1, 6-17]

Light has played a key role in the achieving spatiotemporal control desired for the control of biological systems.[18] Classically, these processes are activated through excitation with UV or short wavelength light. Photocaging[19, 20] and photoaffinity labeling[21] have become staples for modulating and probing the activity of small molecules. Additionally, photochemical switches have been used to reversibly modulate a biological response.[22] For example, azobenzene analogs of the natural product combretastatin CA-4 have been developed as photoswitchable probes of tubulin binding.[23] Light has also been used to regulate the activity of enzymes, providing control over protein assembly in engineered cells.[24]

The bioorthogonal chemistry of tetrazines has become increasingly important across a range of applications in chemical biology, imaging, medicine and materials science.[25, 26] Stoichiometric, "click-to-release" chemistry based on tetrazine-*trans*-cyclooctene ligation was initially described by Robillard and coworkers and has since found broad application for the temporally controlled release of biologically active small molecules.[27-45] Aryl vinylethers have been used in conjunction with tetrazines to release phenols and alcohols.[32, 34, 39] This approach has the advantage of simpler synthetic access but proceeds at rates that are slower than the *trans*-cyclooctene counterpart.

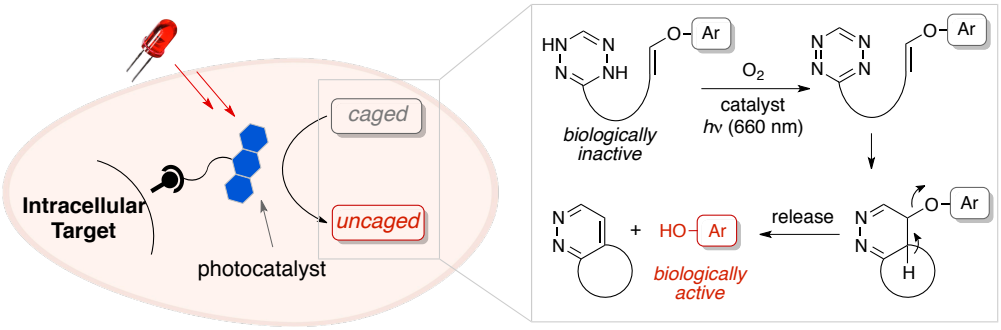

Fig 1. Graphical depiction of subcellularly-localized photocatalysis in conjunction with far-red light. Photocatalytic activation of photocage initiates a cascade of dihydrotetrazine oxidation, intramolecular Diels-Alder reaction, and aromatization to release a biologically active phenol.

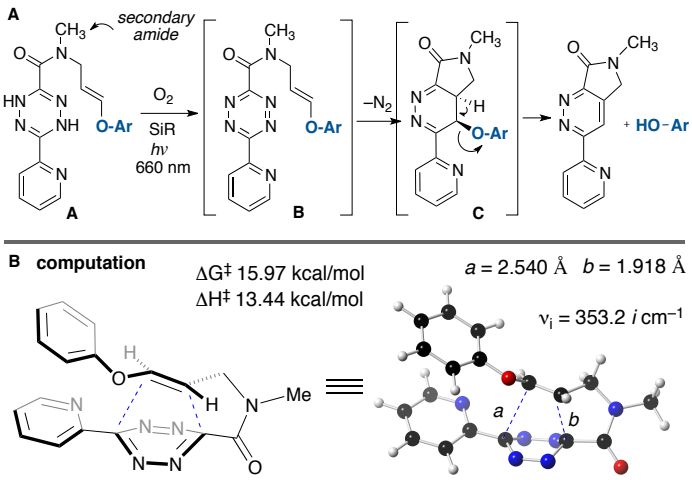

Fig 2. (A) Design of DHTz-Vinylether photocages of structure **A** which upon oxidation under photocatalytic conditions sequentially produce a tetrazine **B** and Diels-Alder adduct **C**. Elimination-aromatization uncage a phenol and produce a pyridazine byproduct. (B) Computation of the transition state for the Diels-Alder reaction of **B** at the M06L/6(311)+G(d,p) level.

Photoactivatable bioorthogonal chemistry— or 'photoclick chemistry'— has emerged as a tool for labeling biological molecules.[46] Prominent examples include conjugations initiated by the photolysis of tetrazole[47] and cyclopropenones,[48] as well as photochemically inducible analogs of the Staudinger[49] and CuAAC[50] reactions as well as cycloadditions involving azirines,[51] benzyne[52], diarylsydnones,[53, 54] quinones,[55-58] *o*-napthaquinone methides[59], *o*-quinodimethanes[60, 61] and *trans*-cycloheptene.[62] Photochemically inducible tetrazine ligation has been described based on methods for uncaging cyclopropene[63, 64] and bicyclononyne[65] dienophiles. Inducible versions of tetrazine ligation have also been described based on the oxidation of dihydrotetrazine (DHTz) precursors[66, 67] Recently, an *o*-nitrophenyl protected dihydrotetrazine has been used with 405 nm light and without catalysis to uncage tetrazines.[68]

The ability to mimic the cellular compartmentalization with non-natural catalysts would provide a unique tool for regulating cellular processes. Recently, several groups have described photocatalytic proximity labeling as a chemoproteomic tool,[69-75] including the use of Ir-photocatalysis has been used to promote azide reduction/uncaging in live cells,[72] where the positively charged Ir-catalyst was non-specifically localized to the negatively charged environment of the mitochondria. Additionally, Ru-photocatalysis in the presence of cells has been used to promote a cellular effect via *E*- to *Z*-isomerization of a combretastatin analog.[76] In this study, neither the substrate nor catalyst were directed to a cellular target. Our own group has developed catalytic activation of bioorthogonal chemistry with light (CABL) as a tool for inducing bioorthogonal chemistry in live cells and in vivo.[77-79] In these approaches, photocatalysis and long wavelength light was used to initiate dihydrotetrazine (DHTz) oxidation and thereby activate rapid bimolecular chemistry with a fluorescently-tagged *trans*-cyclooctene. Silarhodamine (SiR) or fluorescein dyes, commonly used as fluorophores, were repurposed as photocatalysts in combination with 660 nm or 470 nm light, respectively.[77, 78] In these studies, the DHTz was anchored to a biological target, and a freely soluble photocatalyst was utilized. Herein, we describe the first *ligand-directed catalysts for the activation of bioorthogonal chemistry, ,* whereby catalytic groups are localized via a tethered ligand either to DNA or to a protein target in the subcellular environment and used to initiate selective, non-natural reactions with spatiotemporal control (Fig 1). A new class of photocage based on intramolecular tetrazine ligation is described and activated at the organelle level in live cells. Here, a far-red silarhodamine photocatalyst is localized to intracellular targets and used to activate a novel photocage for the release of a microtubule-destabilizing agent in living cells. The photocatalytic system uses long wavelength (660 nm) light which is non-toxic and tissue penetrant as necessary for ultimate *in vivo* application.

Results and Discussion

A photocatalytically inducible photocage based on dihydrotetrazine-tetrazine redox chemistry was designed as outlined in Figure 2. DHTz-vinylether of structure **A** was designed to upon oxidation produce tetrazine **B**, which is situated for intramolecular 4+2 cycloaddition to produce adduct **C**. We anticipated that the rate of the intramolecular Diels-Alder reaction of **B** would be rapid, and that the effective molarity could be enhanced by using a secondary amide tether capable of positioning the dienophile in a reactive s-*cis* amide conformation. Elimination of **C** would deliver a phenol and a dihydropyridazine byproduct. DFT calculations were used to predict whether the intramolecular cycloaddition would be feasible (Fig 2B). Computation at the M06L/6(311)+G(d,p) level located a concerted, asynchronous transition state with $\Delta H^{\ddagger}$ 13.44 kcal/mol and $\Delta G^{\ddagger}$ 15.97 kcal/mol. The more advanced nature of the bond formation at vinyl ether Cβ (1.918 Å) relative to Cα (2.540 Å) reflects the polarization of the vinyl ether dienophile in the Diels-Alder transition state.[80]

DHTz-based photoredox cages were synthesized as shown in Figure 3. Compound **1** was designed to release pyridazine **2** and n-CA4, a potent tubulin inhibitor that is an oxazole-analog of the combretastatin natural products.[81] Also synthesized was the model system **3**, which releases phenol upon photocatalytic oxidation/Diels-Alder, and the control compound **4** that lacks the alkene and is therefore unable to engage the tetrazine in Diels-Alder/release chemistry.

The synthesis of **1** was carried out as shown in Figure 3B. In the key step, the vinylether function was installed by the Alder-ene reaction of aryl allylether **7** with ninhydrin.[82, 83] Thus, isocyanide **5** was condensed with aldehyde **6** to produce the allyl substituted n-CA4 analog **7**.[81] The ene reaction with ninhydrin gave vinyl ether **8** with 4:1 *E*/*Z* selectivity; an isomeric mixture that was carried through to the final step. Subsequent oxidation with H_5IO_6 produced carboxylic acid **9**.[82, 83] Curtius rearrangement with DPPA produced carbamoyl azide **10**, which could be reduced to the amine **11**.[84, 85] Me_3Al-mediated coupling with ethyl 6-(2-pyridyl)-dihydrotetrazine-3-carboxylate[77] provided DHTz-caged n-CA4 analog **1** as a single *E*-stereoisomer after flash chromatography. An analogous sequence was used to produce the model compound **3** from allyl phenyl ether. Also prepared was control compound **4**, a dihydro-analog of **1** that lacks the alkene group and therefore cannot undergo intramolecular Diels-Alder reaction to release nCA-4. Shown in Figure 3C are the structures of commercially available SiR-dyes. As shown for the parent **SiR**, these dyes exist in equilibrium between the more cell

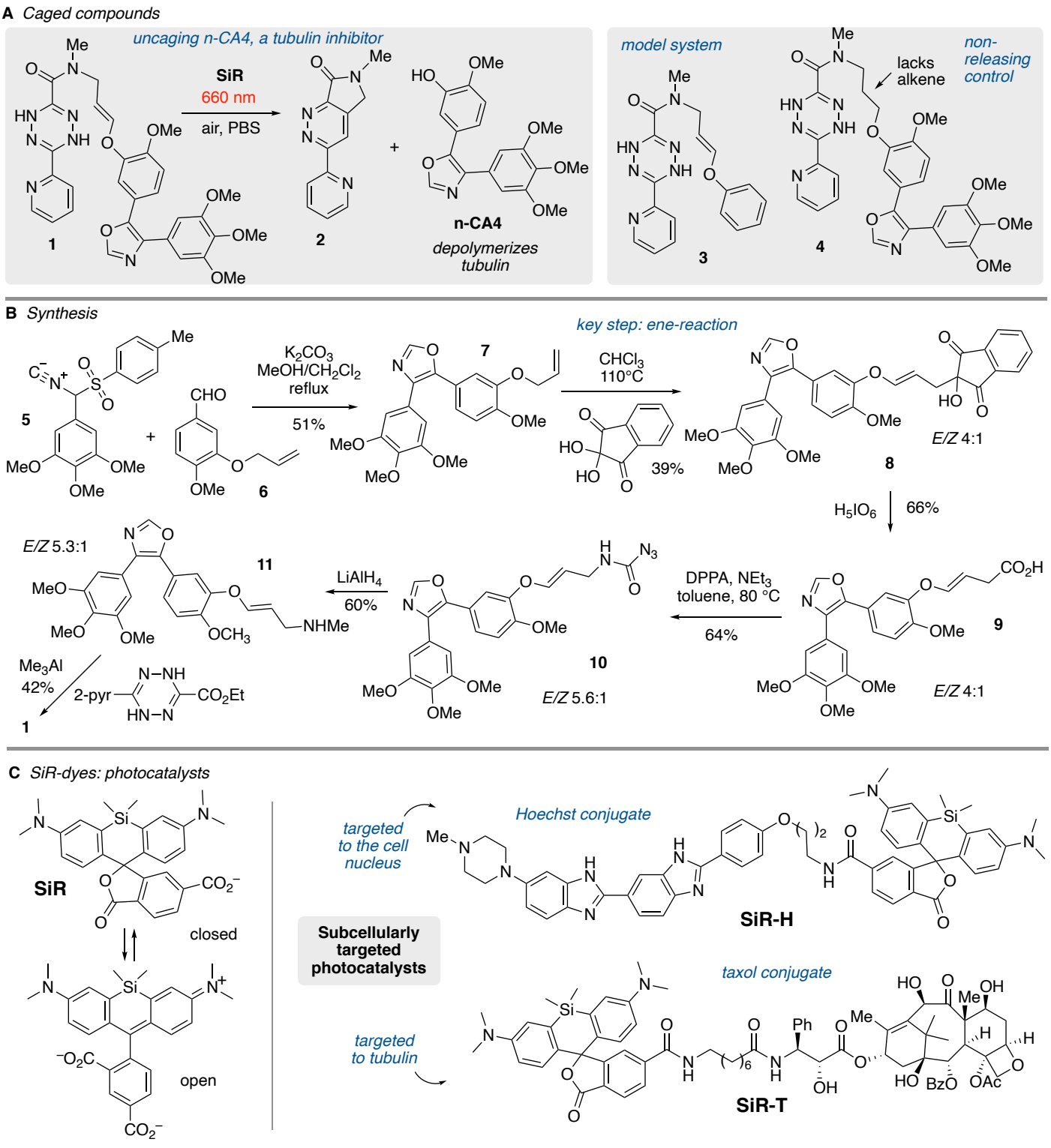

Fig 3. (A) Cage compounds and controls for photocatalytic activation of uncaging based on intramolecular tetrazine ligation. (B) Synthesis of photocage **1** using a ninhydrin Alder-ene reaction to install the aryl vinylether functionality in the key step. (C) Structures of SiR-dyes used as far-red photocatalysts.

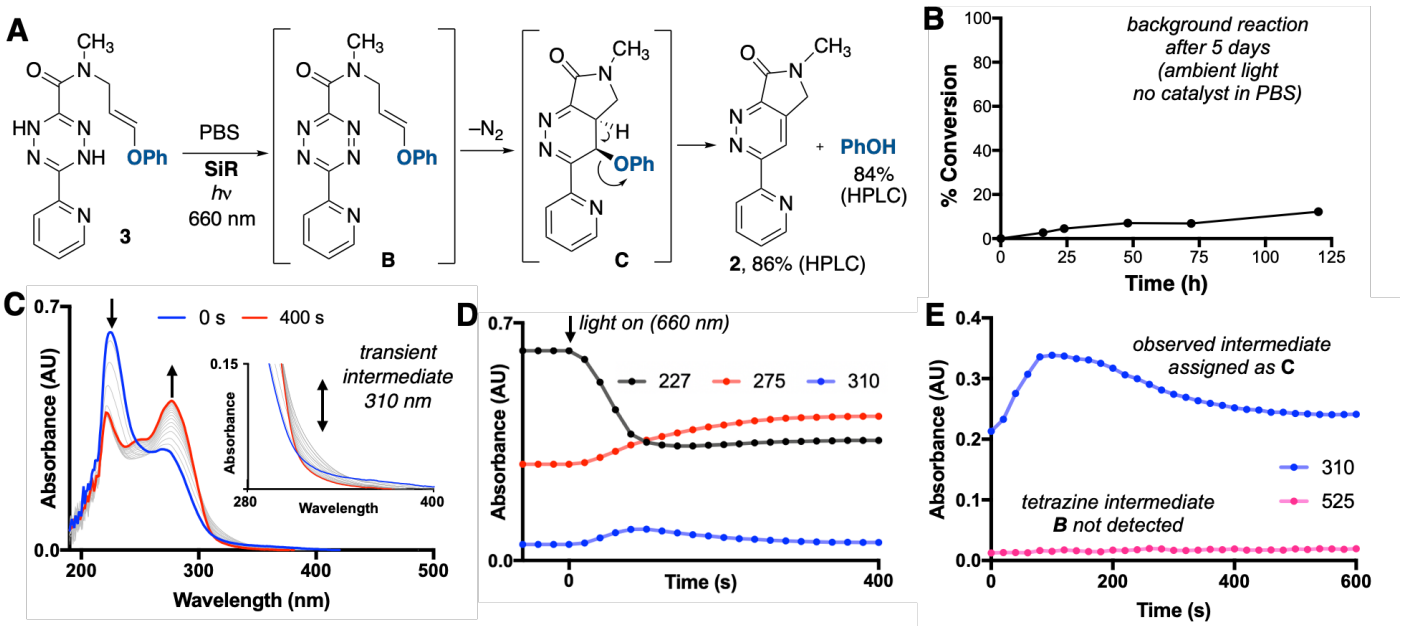

Fig 4 Photo-oxidation studies were done by UV-Vis and HPLC using a model compound **3**, SiR, and 660 nm light. (A) Mechanism of uncaging from **3** to release phenol. By HPLC, the yields of **2** and phenol are 86% and 84% respectively. (B) Stability of **3** in PBS. (C) Whole UV spectra of photo-oxidation of **3** (40 μM) with SiR (2 μM) and red light (660 nm, 400 mW/cm^2) over 400 s. Inset: increase and decrease in 310 nm absorbance for transient intermediate. (D) Absorbance at 227 nm decreases as soon as light turns on. Trace for 310 nm shows increase and decrease in absorbance. Steady increase at 275 nm (**2**). (E) Long pathlength cuvette experiment to better observe intermediates. No change in 525 nm absorbance (intermediate B). Same increase and decrease in 310 nm absorbance observed (intermediate C).

permeable closed-form and the chromophoric open-form. The SiR-Hoechst conjugate **SiR-H** derivative targets the chromophore to DNA in the cell nucleus,[86] and the SiR-Taxol conjugate **SiR-T** targets the chromophore to tubulin.[87]

Photocatalytic oxidation and uncaging studies using model compound **3** were monitored using UV-Vis and HPLC analyses (**Fig 4**). In the presence of **SiR** (2 μM, 5 mol%), irradiation of **3** (40 μM) by 660 nm light for 20 mins lead to the release of **2** and phenol. The yields of the products by HPLC were 86% and 84% respectively (**Fig 4A** and S6). Stability toward background conversion for compound **3** at room temperature without photocatalyst present was tested in chelex-filtered PBS.[88] After 5 days, **3** showed only 15% conversion exhibiting good stability for cellular studies (**Fig 4B**).

Uncaging was monitored by using UV-Vis spectroscopy every 20 seconds to track the presence of starting material, intermediates, and products (**Fig 4C**). In a cuvette, a PBS solution containing **3** (40 μM) and **SiR** (2 μM) was irradiated with 660 nm light until uncaging was complete. Compound **3** absorbs with a UV-vis maximum at 227 nm, and pyridazine product **2** absorbs with a UV-maximum of 275 nm. UV-vis spectral monitoring was carried out during the course of the photochemical reaction, and showed a decrease in absorbance at 227 nm due to the conversion of **3** with concomitant increase in absorption at 275 nm (Fig 4C,D). Transiently, absorption at 310 nm increases and then decreased over the course of the experiment, consistent with the formation of an intermediate. The absorption due to this intermediate reached a maximum after 80 seconds (blue line in Fig 4D,E), and decayed with a half-life of ~100 seconds.

A Diels-Alder/elimination mechanism is proposed for the conversion of **3** to **2**, and we sought to determine if the transient intermediate observed was tetrazine **B** or Diels-Alder cycloadduct **C** (or a tautomer of **C**). Tetrazines typically display a weak, long wavelength absorption due to the tetrazine n-π* transition, providing a spectroscopic handle for distinguishing intermediate **B**. *N*-Butyl 6-(2-pyridyl)-dihydrotetrazine-3-carboxamide,[77] an analog of **B** that lacks the vinylether group, displays an absorption at 525 nm with ε ~450. Due to the low absorptivity expected for **B**, a long pathlength (5 cm) cuvette was used to monitor the photochemical conversion of **3** to **2**. Under these conditions, tetrazine intermediate **B** would be expected to show absorbance of 0.09 AU at 525 nm. Over the course of the reaction, a significant increase and then decrease in absorbance at 310 nm was again observed. However, no change in absorbance at 525 nm was observed (Fig 4C), suggesting that the tetrazine is short lived and the intramolecular reaction occurs faster than is detectable by UV-Vis monitoring. This also means that the intermediate absorbing at 310 nm is intermediate **C** (**Fig 4E**).

We next demonstrated photocatalytic uncaging of n-CA4 with a cellularly-localized catalyst. Uncaging of **1** was analyzed using HPLC. In the presence of **SiR** (5 uM, 10 mol%) and irradiation with 660 nm/220 mW/cm^2 light for 20 mins, yields of **2** and nCA4 were 94% and 39% respectfully (Fig 5). A number of small peaks were

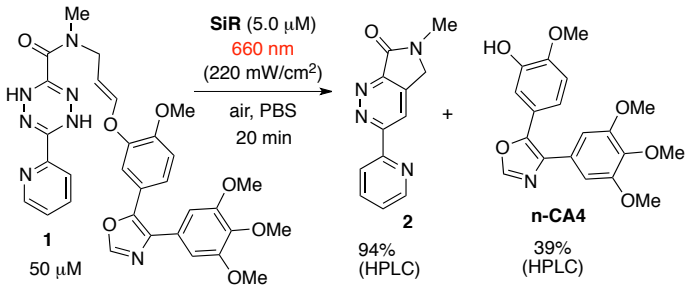

Fig 5. Photocatalytic oxidation/uncaging releases **n-CA4** and **2** at low catalyst concentration. Confirm light power density.

observed along the baseline of the HPLC trace. The modest yield of n-CA4, an electron rich phenol, is due in part to product degradation under the photocatalytic reaction conditions: independent irradiation of 50 μM n-CA4 for 20 min at 660 nm (220 mW cm^2) with SiR (5.0 μM) led to 45% degradation and a similar HPLC profile (Fig S8A). However, degradation was far worse with dyes that produce singlet oxygen in high quantum yield. For example, 5 μM $Ru(bipy)_3(PF_6)_2$ with 470 nm (220 mW/cm^2) light completely degraded 50 μM n-CA4 after 20 min (Fig S8B). With SiR, the uncaging reactions of **1** and **3** proceeded at low catalyst loadings (2-5 μM), prompting us to study if uncaging could be promoted with photocatalysts localized to targets in live cells.

To study the intracellular uncaging of n-CA4, we treated NIH3T3 mouse fibroblasts with **1** and a nuclear- localized **SiR-H** photocatalyst. NIH3T3 cells were chosen because they display elongated tubulin structures making uncaging of a tubulin depolymerizing agent evident and readily quantified. Figure 6 shows a high magnification image of cells that were treated with n-CA4 compared to vehicle. The untreated cells display elongated tubulin fibrils, whereas in the nCA4 treated cells, smaller, bundled tubulin structures are observed. As a result of the collapse of the tubulin cytoskeleton, the nCA4 treated cells show a significant loss in average cell area. To study if a localized, subcellular catalyst could initiate uncaging, we first localized the photocatalyst to the cell nucleus with the silarhodamine-Hoechst dye conjugate **SiR-H**. Following a 2 hour incubation with 500 nM **SiR-H**, unbound photocatalyst was washed away and cells were imaged to verify localization of **SiR-H** to the nucleus (Fig S9B). Cells were then treated with either **1** (25 nM), **4** (25 nM), or n-CA4 (10 nM), and then were irradiated with 660 nm light for 20 mins to initiate uncaging. The lower concentration of n-CA4 (10 nM) used in controls was based on the release yield observed *in vitro* from **1** (Fig 5). Following irradiation, cells were washed once and incubated an additional 25 mins in the dark to allow time for n-CA4 to promote tubulin depolymerization. Cells were then fixed, stained, and imaged to visualize tubulin structures. Controls were performed in cells that were not treated with **SiR-H**, and in cells that were incubated with **SiR-H** in the dark for 20 mins instead of irradiated with 660 nm light (Fig 7A).

Images shown in Figures 6 and 7 depict tubulin in green (antibody stained AF488) and in Figure 7 nuclei are in depicted in blue (DAPI). For the vehicle control (0.1% DMSO in DPBS), cells exhibit elongated, polymerized, and organized tubulin structures, shown in Fig 7B (left) and in high magnification in Fig 6A. Upon treatment with n-CA4 (10 nM), cells display a collapse of the tubulin cytoskeleton and a reduction in cell area [Fig 7B (middle)]. The dramatic change in cell morphology for n-CA4-effected cells is shown in high magnification in Fig 6B. Similarly, cells treated with uncaging conditions [**1** (25 nM) + **SiR-H** + light) exhibit depolymerized tubulin consistent with successful uncaging of n-CA4 (10 nM expected based on a 39% release yield) as shown in Fig 7B (right). For quantification, cells were imaged at 4x magnification, and object area analysis was performed using BioTek Gen5 software in order to measure cellular area relative to cell nuclei (Fig S10). The average area of the tubulin (green) was divided by the average area of the nucleus (blue) for each image to calculate average cell area. The average area for each sample was then normalized to that of the vehicle control for that biological replicate, and the percent

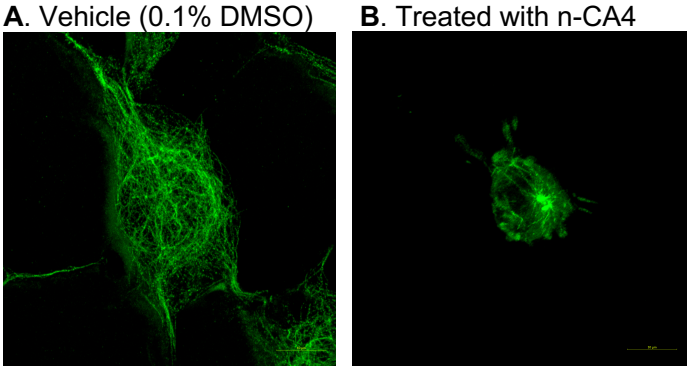

Fig 6. High magnification images of representative NIH 3T3 cells (A) without and (B) with **n-CA4**. After treatment, cells were incubated for 45 min, and were subsequently fixed, antibody stained with AF488, and imaged by confocal microscopy (63.1x magnification with 2x zoom). Scale bars 10 μM

difference between the sample and vehicle was plotted (Fig 7C). Data with negative values signify a decrease in cell area relative to the vehicle control implying tubulin depolymerization, while data at or around zero indicates little change in cell area. Cells treated with n-CA4 regardless of light irradiation displayed a 20% (+/– 4.2%) decrease in cell area compared to the vehicle. Similarly, a 21% (+/– 3.0%) decrease in area was observed for cells treated under uncaging conditions (**1** + **SiR-H** + light). In the absence of light or photocatalyst, **1** does not have a significant effect on cell area. Cells treated with **4**, which lacks the alkene essential for release, do not show a change in cell area with or without photocatalyst and/or light. Additionally, irradiation with **SiR-H** alone does not impact cell area and is not toxic towards cells (Fig S9). These results indicate that the decrease in cell area for **1** + **SiR-H** + light is due to the successful localized uncaging of nCA4 from **1**. Control images for cells treated with conditions that should not induce uncaging (either lacking light, **SiR-H**, or alkene) are shown in Figure 7D. Cells display elongated and organized tubulin similar to that of the vehicle control (Fig 7B(left)) as expected.

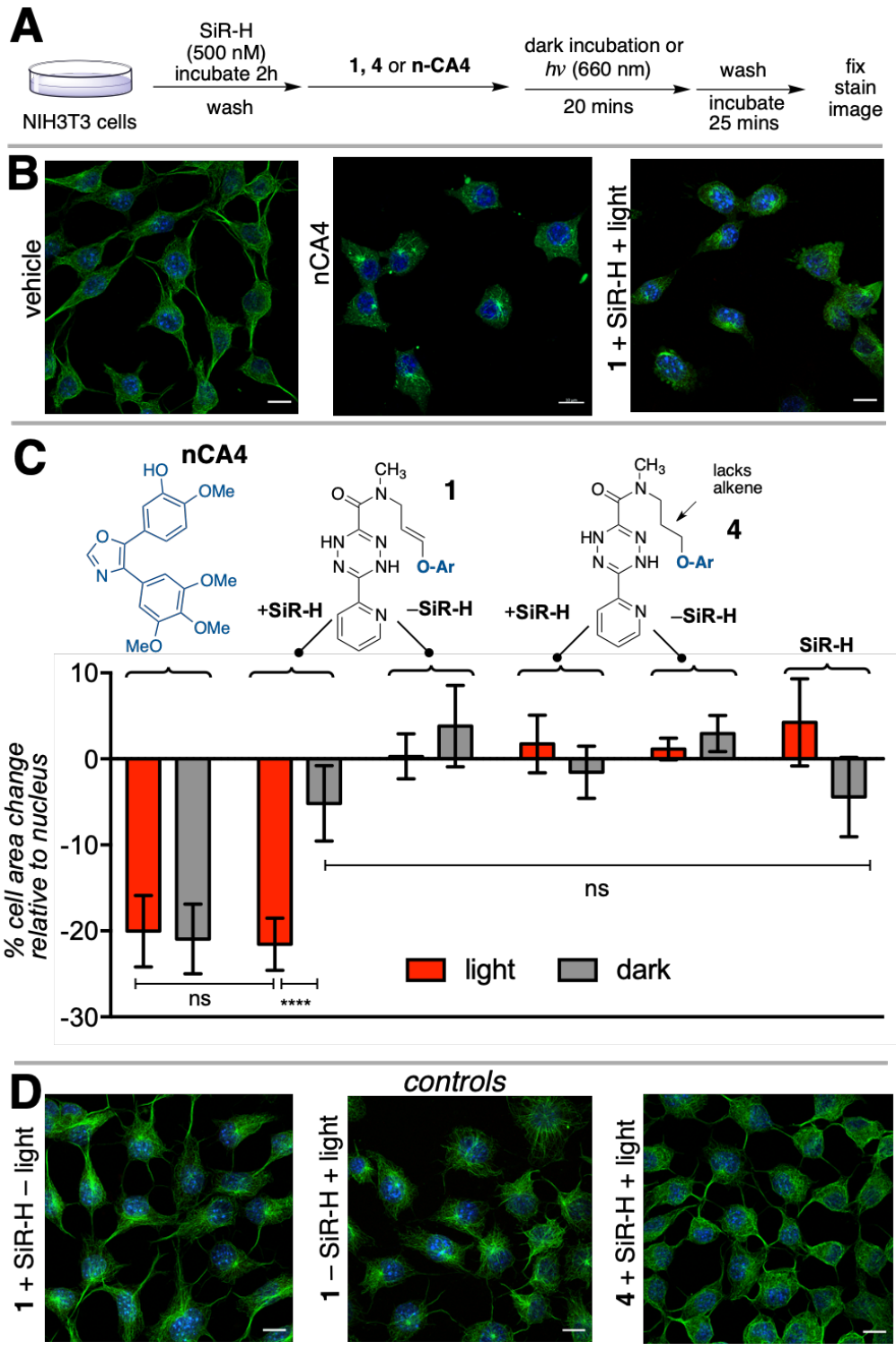

Fig 7 (A) Workflow for localized subcellular uncaging. **SiR-H** localized to the nucleus. (B) Fixed cell images. Green: AF488 antibody (tubulin), Blue: DAPI (nucleus). (C) Quantification of cell area calculated using average tubulin area divided by average nucleus area. Cell areas normalized to that of the vehicle for that data set (biological replicate). "0" indicates average area of vehicle. A significant decrease in cell area was observed upon treatment with nCA4 or uncaging conditions (**1** + **SiR-H** + light). No significant change in area for non-releasing conditions. Red bars (light) irradiated with 660 nm light 20 mins. (D) Fixed cell images of controls. Green: AF488 antibody (tubulin), Blue: DAPI (nucleus). Scale bars 10 μM.

Because **SiR-H** is a reversible binder of DNA (K_D of 8.4 μM),[86] we sought to rule out the possibility that unbound **SiR-H** was promoting photocatalytic uncaging of **3** in the extracellular environment. In order to prove that uncaging is occurring due to the subcellular localization of **SiR-H**, ascorbate was used as an extracellular quencher of photocatalysis. Intracellularly localized **SiR-H** would be unaffected by ascorbate, which is poorly cell permeable,[89] and successful uncaging would still be observed (Fig 8A). However, a cell-impermeable SiR-derivative would be quenched by ascorbate and uncaging would not be expected to occur (Fig 8B).

Excess ascorbate quenches the ability of **SiR** to photocatalyze the oxidation of **3** as shown by UV-Vis with *in situ* irradiation (Fig S4). Ascorbate was also shown to quench SiR-catalyzed oxidation of a dipyridylDHTz analog to its corresponding tetrazine (Fig S4). **SiR** was conjugated to a high molecular weight HA polymer (40 KDa) to create **SiR-X**: an extracellular and impermeable version of the photocatalyst (Fig 8D). Confocal microscopy showed that **SiR-X** is excluded from live 3T3 cells (Fig S13). In the absence of ascorbate, **SiR-X** was shown to catalyze conversion of **3** by UV-Vis when irradiated with 660 nm light (Fig S4). For cellular experiments, we hypothesized that the extracellular ascorbate would quench the ability of extracellular **SiR-X** to photocatalyze uncaging of **3**. Conversely, we anticipated that poorly-permeable ascorbate would *not* quench **SiR-H** which retains photocatalytic activity in the *intracellular* environment.

Cells were treated with either **SiR-H** or **SiR-X** (500 nM), ascorbate (2 mM), and **1** (25 nM) or nCA4 (10 nM) and all samples were irradiated with 660 nm light for 20 mins. Again, the lower concentration of n-CA4 (10 nM) used in controls was based on the release yield observed *in vitro* from **1** (Fig 5). Cells treated with ascorbate alone displayed elongated tubulin structures while treatment with nCA4 and ascorbate led to depolymerized tubulin. In

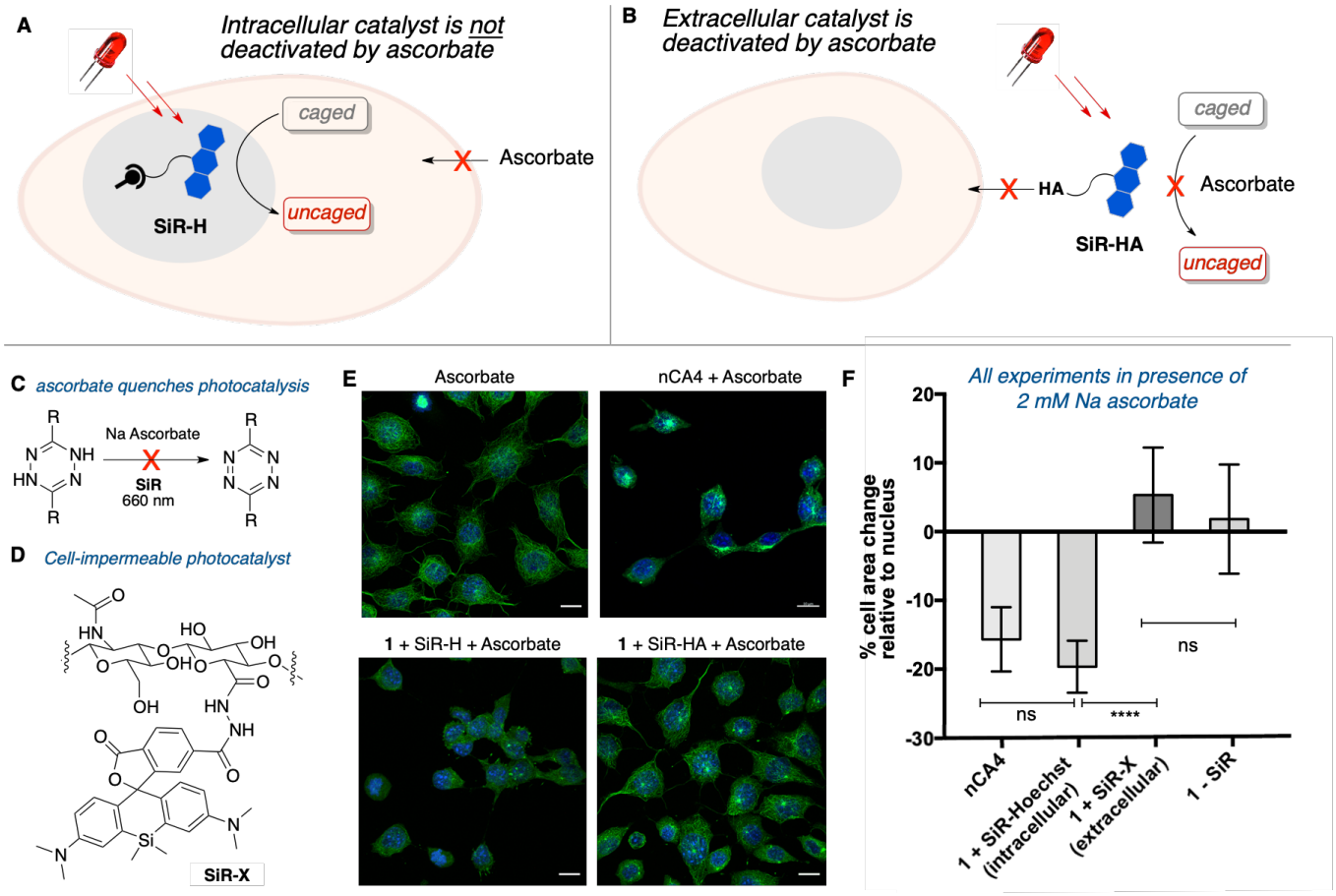

Fig 8 Experiments showing that photocatalytic uncaging takes place intracellularly. Ascorbate deactivates extracellular photocatalysis. (A) Intracellular uncaging should be unaffected by extracellular ascorbate, which has low permeability. (B) Extracellular photocatalyst will not induce uncaging in presence of ascorbate. (C) Ascorbate quenches DHT oxidation (see also Fig S4). (D) Structure of the extracellular photocatalyst **SiR-X**. (E) Fixed cell images. Conditions indicated, all treated with 2 mM ascorbate and irradiated with 660 nm light for 20 mins. In uncaging experiments, the concentration of **1** was 25 nM. Scale bars 10 μM. (F) Quantification of cell area. Similar to the nCA4 control, a significant decrease in cell area is observed for cells irradiated after treatment with **1** + intracellular photocatalyst **SiR-H**, indicating that uncaging is due to localized photocatalyst. A decrease in cell area is not observed in photochemical experiments with **1** and the extracellular catalyst **SiR-X**, or in a control where photocatalyst is omitted.

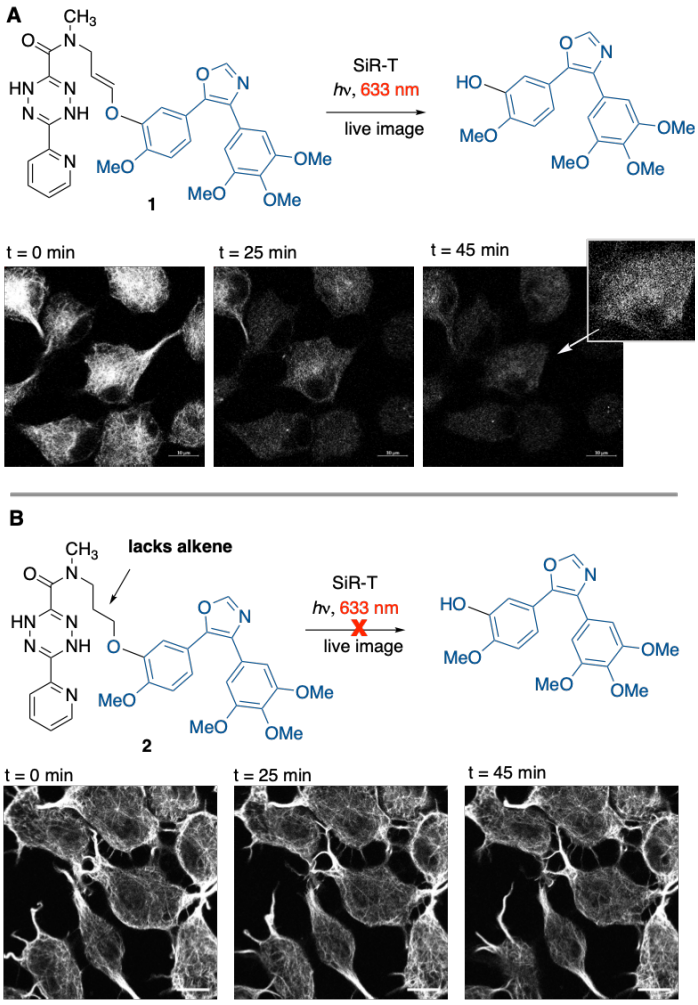

Fig 9 Live cell images of uncaging with photocatalyst localized to tubulin (SiR-T). Illumination at 633 nm activates SiR-T, which serves both as a photocatalyst and fluorescent reporter. The 633 nm laser of the confocal microscope serves the dual purpose of activating the fluorescence and the photocatalytic activity of the SiR-T dye. (A) SiR-T (500 nM) and **1** (25 nM) were added to cells. Cells were illuminated and imaged every 5 mins for 45 mins. Images at 0, 25, and 45 mins show gradual deolymerization of tubulin due to uncaging, characterized by losses in cell area, brightness, and fibrillar structure. Inset: Brightness increased 200%, 1.5x zoom in on single cell to show morphological change. (B) SiR-T (500 nM) and **4** (25 nM) were added to cells. Images were taken every 5 mins for 45 mins. Images at 0, 25, and 45 mins show no change in tubulin. Lack of alkene prevents uncaging. Scale bars 10 μM.

the presence of ascorbate, **1** + **SiR-H**, which localizes to the nucleus, displayed depolymerized tubulin as consistent with successful uncaging (Fig 8E). However under the same conditions, treatment with **1** + **SiR-X**, the cell-impermeable photocatalyst, did not lead to depolymerization of tubulin. The deactivation of **SiR-X** is consistent with the quenching of extracellular photocatalysis by ascorbate, and the persistence of photocatalyzed tubulin depolymerization with **SiR-H** in the presence of ascorbate is consistent with an active, photocatalyst that is localized to the intracellular environment. These conclusions are further supported by cell area quantification data (Fig 8F). Similar to cell studies described above, cell area for the samples treated with ascorbate was calculated. A significant decrease in cell area was seen for cells treated with nCA4 or with **1** + **SiR-H**, the intracellularly localized photocatalyst. However, cells treated with **1** + **SiR-X** or **1** alone exhibited no change in cell area relative to the vehicle control. Again these results suggest successful uncaging due to subcellular photocatalysis.

Finally, confocal microscopy was used to visualize tubulin depolymerization as the result of photocatalytic uncaging in real time in cells that were imaged while live. To do this, we took advantage of the properties of SiR to serve as both a photocatalyst and a fluorophore. By localizing SiR to the tubulin (**SiR-T**), we were able to image the tubulin and initiate uncaging with the 633 nm laser of the confocal microscope. Cells were incubated with **SiR-T** (500 nM) for at least 2 hours before washing and incubating with **1**. Immediately following addition of **1**, cells were imaged every 5 mins for 45 mins. Over this time, steady depolymerization of tubulin can be observed (Fig 9A and Supplementary Movie File). After 45 mins the tubulin structures diminished and there was a loss of the elongated structure seen in normal tubulin.

We also looked at the real time effect of **4** with **SiR-T**. The lack of alkene on **4** prevents uncaging from occurring and we see normal tubulin throughout the 45 min treatment (Fig 9B and Supplementary Movie File). As additional controls, the same experiment was repeated without the addition of **1** or **4** and no change in tubulin structure was observed. Finally, cells were treated with **SiR-T** and were imaged before the addition of **1** and were not imaged again until 45 mins following addition. This serves as a control without light irradiation (Fig S12). No change in tubulin structure was seen in this control experiment demonstrating that light irradiation is necessary for uncaging and that **1** alone does not affect tubulin structure.

Conclusions

In summary, ligand-directed catalysis has been demonstrated for the photocatalytic activation of bioorthogonal chemistry in live cells. Commercially-available SiR-conjugates of Hoechst and Taxol were used to localize **SiR** to the nucleus and tubulin, respectively, and a new class of redox-activated photocage was used to release n-CA4, a microtubule-destabilizing agent. Spectroscopic studies support a mechanism involving rapid intramolecular Diels-Alder reaction and a rate determining elimination step. Uncaging n-CA4 causes microtubule depolymerization and an accompanying reduction in cell area, and control experiments show that uncaging takes place inside the cell, and not in the extracellular environment. With **SiR-T**, the same dye serves as photocatalyst and the fluorescent reporter for tubulin depolyerization, and with confocal microscopy it was possible to visualize tubulin depolymerization in real time as the result of photocatalytic uncaging in live cells.

SUPPORTING INFORMATION

Synthetic procedures and compound characterization data; Spectral studies and kinetics of photooxidation and uncaging; Photostability and Toxicity studies; Live cell imaging and quantification of cell area upon uncaging. A

video file shows the live cell uncaging experiments and controls displayed in Figure 9.

The Supporting Information is available free of charge on the ACS Publications website. The file type is PDF.

AUTHOR INFORMATION

Corresponding Authors

* jmfox@udel.edu

ACKNOWLEDGMENT

This work was supported by NIH (R01GM132460) and Pfizer. Instrumentation was supported by NIH awards P20GM104316, P20GM103446, S10OD025185, S10OD026951, S10OD016267, S10 OD016361, and S10 OD30321. Facilities and instrumentation were also supported by NSF through the University of Delaware Materials Research Science and Engineering Center, DMR-2011824.

References

(1) Rebelein, J. G.; Ward, T. R. In vivo catalyzed new-to-nature reactions. *Curr. Opin. Biotechnol.* **2018**, *53*, 106-114
(2) Sharma, S. K.; Bagshawe, K. D. Antibody Directed Enzyme Prodrug Therapy (ADEPT): Trials and tribulations. *Adv. Drug. Deliv. Rev.* **2017**, *118*, 2-7
(3) Shabat, D.; Lode, H. N.; Pertl, U.; Reisfeld, R. A.; Rader, C.; Lerner, R. A.; Barbas, C. F., 3rd. In vivo activity in a catalytic antibody-prodrug system: Antibody catalyzed etoposide prodrug activation for selective chemotherapy. *Proc. Natl. Acad. Sci. USA* **2001**, *98*, 7528-7533
(4) Sheikh, S.; Ernst, D.; Keating, A. Prodrugs and prodrug-activated systems in gene therapy. *Mol. Ther.* **2021**, *29*, 1716-1728
(5) Gardner, T. J.; Lee, J. P.; Bourne, C. M.; Wijewarnasuriya, D.; Kinarivala, N.; Kurtz, K. G.; Corless, B. C.; Dacek, M. M.; Chang, A. Y.; Mo, G.; Nguyen, K. M.; Brentjens, R. J.; Tan, D. S.; Scheinberg, D. A. Engineering CAR-T cells to activate small-molecule drugs in situ. *Nat. Chem. Biol.* **2022**, *18*, 216-225
(6) Nguyen, D. P.; Nguyen, H. T. H.; Do, L. H. Tools and Methods for Investigating Synthetic Metal-Catalyzed Reactions in Living Cells. *ACS Catal.* **2021**, *11*, 5148-5165
(7) Latocheski, E.; Dal Forno, G. M.; Ferreira, T. M.; Oliveira, B. L.; Bernardes, G. J. L.; Domingos, J. B. Mechanistic insights into transition metal-mediated bioorthogonal uncaging reactions. *Chem. Soc. Rev.* **2020**, *49*, 7710-7729
(8) Martinez-Calvo, M.; Couceiro, J. R.; Destito, P.; Rodriguez, J.; Mosquera, J.; Mascarenas, J. L. Intracellular Deprotection Reactions Mediated by Palladium Complexes Equipped with Designed Phosphine Ligands. *ACS Catal.* **2018**, *8*, 6055-6061
(9) Miller, M. A.; Askevold, B.; Mikula, H.; Kohler, R. H.; Pirovich, D.; Weissleder, R. Nano-palladium is a cellular catalyst for in vivo chemistry. *Nat. Commun.* **2017**, *8*,
(10) Tomas-Gamasa, M.; Martinez-Calvo, M.; Couceiro, J. R.; Mascarenas, J. L. Transition metal catalysis in the mitochondria of living cells. *Nat. Commun.* **2016**, *7*, 12538
(11) Li, J.; Chen, P. R. Development and application of bond cleavage reactions in bioorthogonal chemistry. *Nat. Chem. Biol.* **2016**, *12*, 129-137
(12) Tonga, G. Y.; Jeong, Y. D.; Duncan, B.; Mizuhara, T.; Mout, R.; Das, R.; Kim, S. T.; Yeh, Y. C.; Yan, B.; Hou, S.; Rotello, V. M. Supramolecular regulation of bioorthogonal catalysis in cells using nanoparticle-embedded transition metal catalysts. *Nat. Chem.* **2015**, *7*, 597-603
(13) Volker, T.; Dempwolff, F.; Graumann, P. L.; Meggers, E. Progress towards bioorthogonal catalysis with organometallic compounds. *Angew. Chem. Int. Edit.* **2014**, *53*, 10536-10540
(14) Li, J.; Yu, J.; Zhao, J.; Wang, J.; Zheng, S.; Lin, S.; Chen, L.; Yang, M.; Jia, S.; Zhang, X.; Chen, P. R. Palladium-triggered deprotection chemistry for protein activation in living cells. *Nat. Chem.* **2014**, *6*, 352-361
(15) Chankeshwara, S. V.; Indrigo, E.; Bradley, M. Palladium-mediated chemistry in living cells. *Curr. Opin. Chem. Biol.* **2014**, *21*, 128-135
(16) Yusop, R. M.; Unciti-Broceta, A.; Johansson, E. M.; Sanchez-Martin, R. M.; Bradley, M. Palladium-mediated intracellular chemistry. *Nat. Chem.* **2011**, *3*, 239-243
(17) Streu, C.; Meggers, E. Ruthenium-induced allylcarbamate cleavage in living cells. *Angew. Chem. Int. Edit.* **2006**, *45*, 5645-5648
(18) Ankenbruck, N.; Courtney, T.; Naro, Y.; Deiters, A. Optochemical Control of Biological Processes in Cells and Animals. *Angew. Chem. Int. Edit.* **2018**, *57*, 2768-2798
(19) Klan, P.; Solomek, T.; Bochet, C. G.; Blanc, A.; Givens, R.; Rubina, M.; Popik, V.; Kostikov, A.; Wirz, J. Photoremovable protecting groups in chemistry and biology: reaction mechanisms and efficacy. *Chem. Rev.* **2013**, *113*, 119-191
(20) Gostl, R.; Senf, A.; Hecht, S. Remote-controlling chemical reactions by light: towards chemistry with high spatio-temporal resolution. *Chem. Soc. Rev.* **2014**, *43*, 1982-1996
(21) Mishra, P. K.; Yoo, C. M.; Hong, E.; Rhee, H. W. Photo-crosslinking: An Emerging Chemical Tool for Investigating Molecular Networks in Live Cells. *ChemBioChem* **2020**, *21*, 924-932
(22) Hull, K.; Morstein, J.; Trauner, D. In Vivo Photopharmacology. *Chem. Rev.* **2018**, *118*, 10710-10747
(23) Borowiak, M.; Nahaboo, W.; Reynders, M.; Nekolla, K.; Jalinot, P.; Hasserodt, J.; Rehberg, M.; Delattre, M.; Zahler, S.; Vollmar, A.; Trauner, D.; Thorn-Seshold, O. Photoswitchable Inhibitors of Microtubule Dynamics Optically Control Mitosis and Cell Death. *Cell* **2015**, *162*, 403-411
(24) Shaaya, M.; Fauser, J.; Zhurikhina, A.; Conage-Pough, J. E.; Huyot, V.; Brennan, M.; Flower, C. T.; Matsche, J.; Khan, S.; Natarajan, V.; Rehman, J.; Kota, P.; White, F. M.; Tsygankov, D.; Karginov, A. V. Light-regulated allosteric switch enables temporal and subcellular control of enzyme activity. *Elife* **2020**, *9*,
(25) Wu, H.; Devaraj, N. K. Inverse Electron-Demand Diels-Alder Bioorthogonal Reactions. *Top. Curr. Chem.* **2016**, *374*, 3
(26) Scinto, S. L.; Bilodeau, D. A.; Hincapie, R.; Lee, W.; Nguyen, S. S.; Xu, M.; Am Ende, C. W.; Finn, M. G.; Lang, K.; Lin, Q.; Pezacki, J. P.; Prescher, J. A.; Robillard, M. S.; Fox, J. M. Bioorthogonal chemistry. *Nat. Rev. Methods Primers* **2021**, *1*,
(27) Versteegen, R. M.; Rossin, R.; ten Hoeve, W.; Janssen, H. M.; Robillard, M. S. Click to release: instantaneous doxorubicin elimination upon tetrazine ligation. *Angew. Chem. Int. Edit.* **2013**, *52*, 14112-14116
(28) Li, J.; Jia, S.; Chen, P. R. Diels-Alder reaction-triggered bioorthogonal protein decaging in living cells. *Nat. Chem. Biol.* **2014**, *10*, 1003-1005
(29) Matikonda, S. S.; Orsi, D. L.; Staudacher, V.; Jenkins, I. A.; Fiedler, F.; Chen, J.; Gamble, A. B. Bioorthogonal prodrug activation driven by a strain-promoted 1,3-dipolar cycloaddition. *Chem. Sci.* **2015**, *6*, 1212-1218
(30) Mejia Oneto, J. M.; Khan, I.; Seebald, L.; Royzen, M. In Vivo Bioorthogonal Chemistry Enables Local Hydrogel and Systemic Pro-Drug To Treat Soft Tissue Sarcoma. *ACS Central Science* **2016**, *2*, 476-482
(31) Rossin, R.; van Duijnhoven, S. M. J.; ten Hoeve, W.; Janssen, H. M.; Kleijn, L. H. J.; Hoeben, F. J. M.; Versteegen, R. M.; Robillard, M. S. Triggered Drug Release from an Antibody–Drug Conjugate Using Fast "Click-to-Release" Chemistry in Mice. *Bioconj. Chem.* **2016**, *27*, 1697-1706
(32) Wu, H.; Alexander, S. C.; Jin, S.; Devaraj, N. K. A Bioorthogonal Near-Infrared Fluorogenic Probe for mRNA Detection. *J. Am. Chem. Soc.* **2016**, *138*, 11429-11432

(33) Zhang, G.; Li, J.; Xie, R.; Fan, X.; Liu, Y.; Zheng, S.; Ge, Y.; Chen, P. R. Bioorthogonal Chemical Activation of Kinases in Living Systems. *ACS Cent. Sci.* **2016**, *2*, 325-331
(34) Jiménez-Moreno, E.; Guo, Z.; Oliveira, B. L.; Albuquerque, I. S.; Kitowski, A.; Guerreiro, A.; Boutureira, O.; Rodrigues, T.; Jiménez-Osés, G.; Bernardes, G. J. L. Vinyl Ether/Tetrazine Pair for the Traceless Release of Alcohols in Cells. *Angew. Chem. Int. Edit.* **2017**, *56*, 243-247
(35) Carlson, J. C. T.; Mikula, H.; Weissleder, R. Unraveling Tetrazine-Triggered Bioorthogonal Elimination Enables Chemical Tools for Ultrafast Release and Universal Cleavage. *J. Am. Chem. Soc.* **2018**, *140*, 3603-3612
(36) Czuban, M.; Srinivasan, S.; Yee, N. A.; Agustin, E.; Koliszak, A.; Miller, E.; Khan, I.; Quinones, I.; Noory, H.; Motola, C.; Volkmer, R.; Di Luca, M.; Trampuz, A.; Royzen, M.; Mejia Oneto, J. M. Bio-Orthogonal Chemistry and Reloadable Biomaterial Enable Local Activation of Antibiotic Prodrugs and Enhance Treatments against Staphylococcus aureus Infections. *ACS Cent. Sci.* **2018**, 1624-1632
(37) Davies, S.; Stenton, B. J.; Bernardes, G. J. L. Bioorthogonal Decaging Reactions for Targeted Drug Activation. *Chimia* **2018**, *72*, 771-776
(38) Rossin, R.; Versteegen, R. M.; Wu, J.; Khasanov, A.; Wessels, H. J.; Steenbergen, E. J.; ten Hoeve, W.; Janssen, H. M.; van Onzen, A. H. A. M.; Hudson, P. J.; Robillard, M. S. Chemically triggered drug release from an antibody-drug conjugate leads to potent antitumour activity in mice. *Nat. Commun.* **2018**, *9*, 1484
(39) Staderini, M.; Gambardella, A.; Lilienkampf, A.; Bradley, M. A Tetrazine-Labile Vinyl Ether Benzyloxycarbonyl Protecting Group (VeZ): An Orthogonal Tool for Solid-Phase Peptide Chemistry. *Org. Lett.* **2018**, *20*, 3170-3173
(40) Ji, X.; Pan, Z.; Yu, B.; De La Cruz, L. K.; Zheng, Y.; Ke, B.; Wang, B. Click and release: bioorthogonal approaches to "on-demand" activation of prodrugs. *Chem. Soc. Rev.* **2019**, *48*, 1077-1094
(41) Tu, J.; Xu, M.; Franzini, R. M. Dissociative Bioorthogonal Reactions. *ChemBioChem* **2019**, *20*, 1615-1627
(42) van Onzen, A. H. A. M.; Versteegen, R. M.; Hoeben, F. J. M.; Filot, I. A. W.; Rossin, R.; Zhu, T.; Wu, J.; Hudson, P. J.; Janssen, H. M.; ten Hoeve, W.; Robillard, M. S. Bioorthogonal Tetrazine Carbamate Cleavage by Highly Reactive trans-Cyclooctene. *J. Am. Chem. Soc.* **2020**, *142*, 10955–10963
(43) Wilkovitsch, M.; Haider, M.; Sohr, B.; Herrmann, B.; Klubnick, J.; Weissleder, R.; Carlson, J. C. T.; Mikula, H. A Cleavable C2-Symmetric trans-Cyclooctene Enables Fast and Complete Bioorthogonal Disassembly of Molecular Probes. *J. Am. Chem. Soc.* **2020**, *142*, 19132-19141
(44) Kang, D.; Lee, S.; Kim, J. Bioorthogonal click and release: A general, rapid, chemically revertible bioconjugation strategy employing enamine N-oxides. *Chem* **2022**, *8*, 2260-2277
(45) Wang, Y.; Shen, G.; Li, J.; Mao, W.; Sun, H.; Feng, P.; Wu, H. Bioorthogonal Cleavage of Tetrazine-Caged Ethers and Esters Triggered by trans-Cyclooctene. *Org. Lett.* **2022**, *24*, 5293-5297
(46) Kumar, G. S.; Lin, Q. Light-Triggered Click Chemistry. *Chem. Rev.* **2021**, *121*, 6991-7031
(47) Kumar, G. S.; Racioppi, S.; Zurek, E.; Lin, Q. Superfast Tetrazole-BCN Cycloaddition Reaction for Bioorthogonal Protein Labeling on Live Cells. *J. Am. Chem. Soc.* **2022**, *144*, 57-62
(48) Poloukhtine, A. A.; Mbua, N. E.; Wolfert, M. A.; Boons, G.-J.; Popik, V. V. Selective Labeling of Living Cells by a Photo-Triggered Click Reaction. *J. Am. Chem. Soc.* **2009**, *131*, 15769-15776
(49) Shah, L.; Laughlin, S. T.; Carrico, I. S. Light-Activated Staudinger–Bertozzi Ligation within Living Animals. *J. Am. Chem. Soc.* **2016**, *138*, 5186-5189
(50) Shete, A. U.; El-Zaatari, B. M.; French, J. M.; Kloxin, C. J. Blue-light activated rapid polymerization for defect-free bulk Cu(i)-catalyzed azide–alkyne cycloaddition (CuAAC) crosslinked networks. *Chem. Commun.* **2016**, *52* (69), 10574-10577
(51) Lim, R. K. V.; Lin, Q. Azirine ligation: fast and selective protein conjugation via photoinduced azirine–alkene cycloaddition. *Chem. Commun.* **2010**, *46* (42), 7993-7995
(52) Gann, A. W.; Amoroso, J. W.; Einck, V. J.; Rice, W. P.; Chambers, J. J.; Schnarr, N. A. A photoinduced, benzyne click reaction. *Org. Lett.* **2014**, *16* (7), 2003-2005
(53) Gao, J.; Xiong, Q.; Wu, X.; Deng, J.; Zhang, X.; Zhao, X.; Deng, P.; Yu, Z. Direct ring-strain loading for visible-light accelerated bioorthogonal ligation via diarylsydnone-dibenzo[b,f][1,4,5]thiadiazepine photo-click reactions. *Commun. Chem.* **2020**, (1), 29
(54) Zhang, L.; Zhang, X.; Yao, Z.; Jiang, S.; Deng, J.; Li, B.; Yu, Z. Discovery of Fluorogenic Diarylsydnone-Alkene Photoligation: Conversion of ortho-Dual-Twisted Diarylsydnones into Planar Pyrazolines. *J. Am. Chem. Soc.* **2018**, *140* (24), 7390-7394
(55) Li, J.; Kong, H.; Huang, L.; Cheng, B.; Qin, K.; Zheng, M.; Yan, Z.; Zhang, Y. Visible Light-Initiated Bioorthogonal Photoclick Cycloaddition. *J Am Chem Soc* **2018**, *140* (44), 14542-14546
(56) Li, J.; Kong, H.; Zhu, C.; Zhang, Y. Photo-controllable bioorthogonal chemistry for spatiotemporal control of bio-targets in living systems. *Chem. Sci.* **2020**, *11* (13), 3390-3396
(57) Bruins, J. J.; Albada, B.; van Delft, F. ortho-Quinones and Analogues Thereof: Highly Reactive Intermediates for Fast and Selective Biofunctionalization. *Chem. Eur. J.* **2018**, *24* (19), 4749-4756,PMC5900998.
(58) Bruins, J. J.; Blanco-Ania, D.; Van Der Doef, V.; Van Delft, F. L.; Albada, B. Orthogonal, dual protein labelling by tandem cycloaddition of strained alkenes and alkynes to ortho-quinones and azides. *Chem. Commun.* **2018**, *54* (53), 7338-7341
(59) Arumugam, S.; Popik, V. V. Photochemical Generation and the Reactivity ofo-Naphthoquinone Methides in Aqueous Solutions. *J. Am. Chem. Soc.* **2009**, *131* (33), 11892-11899
(60) Feist, F.; Rodrigues, L. L.; Walden, S. L.; Krappitz, T. W.; Dargaville, T. R.; Weil, T.; Goldmann, A. S.; Blinco, J. P.; Barner-Kowollik, C. Light-induced Ligation of o-Quinodimethanes with Gated Fluorescence Self-reporting. *J. Am. Chem. Soc.* **2020**, *142* (17), 7744-7748
(61) Bruins, J. J.; Westphal, A. H.; Albada, B.; Wagner, K.; Bartels, L.; Spits, H.; Van Berkel, W. J. H.; Van Delft, F. L. Inducible, Site-Specific Protein Labeling by Tyrosine Oxidation–Strain-Promoted (4 + 2) Cycloaddition. *Bioconj. Chem.* **2017**, *28* (4), 1189-1193
(62) Singh, K.; Fennell, C. J.; Coutsias, E. A.; Latifi, R.; Hartson, S.; Weaver, J. D. Light Harvesting for Rapid and Selective Reactions: Click Chemistry with Strain-Loadable Alkenes. *Chem* **2018**, *4* (1), 124-137
(63) Kumar, P.; Zainul, O.; Camarda, F. M.; Jiang, T.; Mannone, J. A.; Huang, W.; Laughlin, S. T. Caged Cyclopropenes with Improved Tetrazine Ligation Kinetics. *Org. Lett.* **2019**, *21* (10), 3721-3725
(64) Jiang, T.; Kumar, P.; Huang, W.; Kao, W. S.; Thompson, A. O.; Camarda, F. M.; Laughlin, S. T. Modular Enzyme- and Light-Based Activation of Cyclopropene–Tetrazine Ligation. *ChemBioChem* **2019**, *20* (17), 2222-2226
(65) Mayer, S. V.; Murnauer, A.; Wrisberg, M. K.; Jokisch, M. L.; Lang, K. Photo-induced and Rapid Labeling of Tetrazine-Bearing Proteins via Cyclopropenone-Caged Bicyclononynes. *Angew. Chem. Int. Ed.* **2019**, *58* (44), 15876-15882
(66) Ehret, F.; Wu, H.; Alexander, S. C.; Devaraj, N. K. Electrochemical Control of Rapid Bioorthogonal Tetrazine Ligations for Selective Functionalization of Microelectrodes. *J. Am. Chem. Soc.* **2015**, *137* (28), 8876-8879
(67) Nickerl, G.; Senkovska, I.; Kaskel, S. Tetrazine functionalized zirconium MOF as an optical sensor for oxidizing gases. *Chem. Commun.* **2015**, *51* (12), 2280-2282
(68) Liu, L.; Zhang, D.; Johnson, M.; Devaraj, N. K. Light-activated tetrazines enable precision live-cell bioorthogonal chemistry. *Nat. Chem.* **2022**, *14*, 1078-1085

(69) Geri, J. B.; Oakley, J. V.; Reyes-Robles, T.; Wang, T.; McCarver, S. J.; White, C. H.; Rodriguez-Rivera, F. P.; Parker, D. L., Jr.; Hett, E. C.; Fadeyi, O. O.; Oslund, R. C.; MacMillan, D. W. C. Microenvironment mapping via Dexter energy transfer on immune cells. *Science* **2020**, *367* (6482), 1091-1097,PMC7336666.
(70) Tsushima, M.; Sato, S.; Miura, K.; Niwa, T.; Taguchi, H.; Nakamura, H. Intracellular photocatalytic-proximity labeling for profiling protein-protein interactions in microenvironments. *Chem. Commun.* **2022**, *58* (12), 1926-1929
(71) Oslund, R. C.; Reyes-Robles, T.; White, C. H.; Tomlinson, J. H.; Crotty, K. A.; Bowman, E. P.; Chang, D.; Peterson, V. M.; Li, L.; Frutos, S.; Vila-Perelló, M.; Vlerick, D.; Cromie, K.; Perlman, D. H.; Ingale, S.; Hara, S. D. O.; Roberts, L. R.; Piizzi, G.; Hett, E. C.; Hazuda, D. J.; Fadeyi, O. O. Detection of cell-cell interactions via photocatalytic cell tagging. *Nat Chem Biol* **2022**,
(72) Huang, Z.; Liu, Z.; Xie, X.; Zeng, R.; Chen, Z.; Kong, L.; Fan, X.; Chen, P. R. Bioorthogonal Photocatalytic Decaging-Enabled Mitochondrial Proteomics. *J. Am. Chem. Soc.* **2021**, *143*, 18714-18720
(73) Buksh, B. F.; Knutson, S. D.; Oakley, J. V.; Bissonnette, N. B.; Oblinsky, D. G.; Schwoerer, M. P.; Seath, C. P.; Geri, J. B.; Rodriguez-Rivera, F. P.; Parker, D. L.; Scholes, G. D.; Ploss, A.; MacMillan, D. W. C. μMap-Red: Proximity Labeling by Red Light Photocatalysis. *J. Am. Chem. Soc.* **2022**, *144* (14), 6154-6162
(74) Trowbridge, A. D.; Seath, C. P.; Rodriguez-Rivera, F. P.; Li, B. X.; Dul, B. E.; Schwaid, A. G.; Geri, J. B.; Oakley, J. V.; Fadeyi, O. O.; Oslund, R. C.; Ryu, K. A.; White, C.; Reyes-Robles, T.; Tawa, P.; Parker, D. L.; MacMillan, D. W. C. Small molecule photocatalysis enables drug target identification via energy transfer. *bioRxiv* **2021**, 2021.2008.2002.454797
(75) Tay, N.; Ryu, K. A.; Weber, J.; Olow, A.; Reichman, D.; Oslund, R.; Fadeyi, O.; Rovis, T. Targeted Activation in Localized Protein Environments via Deep Red Photoredox Catalysis. *ChemRxiv* **2022**, doi: 10.26434/chemrxiv-22021-x26439bjv
(76) Watson, E. E.; Russo, F.; Moreau, D.; Winssinger, N. Optochemical Control of Therapeutic Agents through Photocatalyzed Isomerization. *Angew. Chem. Int. Edit.* **2022**, *61*, e202203390
(77) Jemas, A.; Xie, Y.; Pigga, J. E.; Caplan, J. L.; am Ende, C. W.; Fox, J. M. Catalytic Activation of Bioorthogonal Chemistry with Light (CABL) Enables Rapid, Spatiotemporally Controlled Labeling and No-Wash, Subcellular 3D-Patterning in Live Cells Using Long Wavelength Light. *J. Am. Chem. Soc.* **2022**, *144*, 1647-1662
(78) Wang, C.; Zhang, H.; Zhang, T.; Zou, X.; Wang, H.; Rosenberger, J. E.; Vannam, R.; Trout, W. S.; Grimm, J. B.; Lavis, L. D.; Thorpe, C.; Jia, X.; Li, Z.; Fox, J. M. Enabling In Vivo Photocatalytic Activation of Rapid Bioorthogonal Chemistry by Repurposing Silicon-Rhodamine Fluorophores as Cytocompatible Far-Red Photocatalysts. *J. Am. Chem. Soc.* **2021**, *143*, 10793-10803
(79) Zhang, H.; Trout, W. S.; Liu, S.; Andrade, G. A.; Hudson, D. A.; Scinto, S. L.; Dicker, K. T.; Li, Y.; Lazouski, N.; Rosenthal, J.; Thorpe, C.; Jia, X.; Fox, J. M. Rapid Bioorthogonal Chemistry Turn-on through Enzymatic or Long Wavelength Photocatalytic Activation of Tetrazine Ligation. *J. Am. Chem. Soc.* **2016**, *138*, 5978-5983
(80) Jasiński, R.; Kubik, M.; Łapczuk-Krygier, A.; Kącka, A.; Dresler, E.; Boguszewska-Czubara, A. An experimental and theoretical study of the hetero Diels–Alder reactions between (E)-2-aryl-1-cyano-1-nitroethenes and ethyl vinyl ether: one-step or zwitterionic, two-step mechanism? *Reaction Kinetics, Mechanisms and Catalysis* **2014**, *113*, 333-345
(81) Wang, L.; Woods, K. W.; Li, Q.; Barr, K. J.; McCroskey, R. W.; Hannick, S. M.; Gherke, L.; Credo, R. B.; Hui, Y.-H.; Marsh, K.; Warner, R.; Lee, J. Y.; Zielinski-Mozng, N.; Frost, D.; Rosenberg, S. H.; Sham, H. L. Potent, Orally Active Heterocycle-Based Combretastatin A-4 Analogues: Synthesis, Structure–Activity Relationship, Pharmacokinetics, and In Vivo Antitumor Activity Evaluation. *J. Med. Chem.* **2002**, *45*, 1697-1711
(82) Gill, G. B.; Idris, M. S. H.; Kirollos, K. S. Ene reactions of indane-1,2,3-trione (a super-enophile) and related vicinal tricarbonyl systems. *J. Chem. Soc., Perkin Trans. 1* **1992**, 2355-2365
(83) Gill, G. B.; Idris, M. S. H.; Kirollos, K. S. Oxidative cleavage of indane-1,2,3-trione-ene adducts; a convenient synthesis of allyl and allenyl carboxylic acids. *J. Chem. Soc., Perkin Trans. 1* **1992**, 2367-2369
(84) Uneyama, K.; Makio, S.; Nanbu, H. Synthesis of organofluorine building blocks. 3. An electrochemical preparation and reaction of dimethyl 2,3-bis(2,2,2-trifluoroethyl)succinate. *J. Org. Chem.* **1989**, *54*, 872-877
(85) Ninomiya, K.; Shioiri, T.; Yamada, S. Phosphorus in organic synthesis—VII: Diphenyl phosphorazidate (DPPA). A new convenient reagent for a modified curtius reaction. *Tetrahedron* **1974**, *30*, 2151-2157
(86) Lukinavičius, G.; Blaukopf, C.; Pershagen, E.; Schena, A.; Reymond, L.; Derivery, E.; Gonzalez-Gaitan, M.; D'Este, E.; Hell, S. W.; Wolfram Gerlich, D.; Johnsson, K. SiR–Hoechst is a far-red DNA stain for live-cell nanoscopy. *Nat. Commun.* **2015**, *6*, 8497
(87) Lukinavičius, G.; Reymond, L.; D'Este, E.; Masharina, A.; Göttfert, F.; Ta, H.; Güther, A.; Fournier, M.; Rizzo, S.; Waldmann, H.; Blaukopf, C.; Sommer, C.; Gerlich, D. W.; Arndt, H.-D.; Hell, S. W.; Johnsson, K. Fluorogenic probes for live-cell imaging of the cytoskeleton. *Nat. Methods* **2014**, *11*, 731-733
(88) The PBS for all studies was demetalated by filtration through chelex resin prior to use.
(89) Hannesschlaeger, C.; Pohl, P. Membrane Permeabilities of Ascorbic Acid and Ascorbate. *Biomolecules* **2018**, *8*, 73